



Water, heat and solute dynamics of a mud boil, Spitsbergen

Julia Boike^{a,*}, Olaf Ippisch^{b,1}, Pier Paul Overduin^{c,2},
Birgit Hagedorn^{d,3}, Kurt Roth^{e,4}

^a Alfred Wegener Institute for Polar and Marine Research, Telegrafenberg A43, 14473 Potsdam, Germany

^b Interdisciplinary Center for Scientific Computing, INF368, University of Heidelberg, 69120 Heidelberg, Germany

^c Water and Environment Research Center, University of Alaska Fairbanks, Fairbanks, AK 99775-5860, USA

^d Quaternary Research Center, University of Washington, Box 351360, Seattle, WA 98195, USA

^e Institute of Environmental Physics, INF 229, University of Heidelberg, 69120 Heidelberg, Germany

Received 17 May 2005; received in revised form 28 October 2005; accepted 9 July 2006

Abstract

Mud boils, a form of non-sorted circles, cover the ground surface in many periglacial landscapes. The vegetation-covered trough acts as an effective buffer to the downward movement of water and chemicals, while the bare center experiences larger fluxes of heat and mass. Since dissolved ions affect the electric conductivity of the soil solution, measurements of the bulk soil electric conductivity offer potential for estimating solute concentration. Since 1998, bulk soil electric conductivity has been measured automatically and hourly using 32 time domain reflectometry probes over an approximately 1 m diameter mud boil close to Ny Ålesund, Spitsbergen. Soil water electric conductivity was calculated from bulk soil electric conductivity using volumetric soil water content and a calibration parameter. The seasonal and spatial behaviour of water, temperature and solute concentration within two profiles of this mud boil were analyzed. Concentrations of estimated soil water electric conductivity were highest during the summer period when the active layer was thawed. Thermodynamic equilibrium modelling of the soil solution during freezing suggests that precipitation of dissolved species leads to the observed decrease in electric conductivity. There is a pronounced vertical solute concentration gradient in both profiles, while there is little evidence for horizontal solute concentration gradients beneath the mudboil.

© 2007 Elsevier B.V. All rights reserved.

Keywords: Permafrost; Freezing; Geophysical methods; Electric conductivity; Solute dynamics; Patterned ground

1. Introduction

Analysis of the phenomenology and dynamic processes of patterned ground yields information on past and present climate and environmental conditions (Washburn, 1979; Romanovskii, 1996). The objective of this study is to characterize (seasonally and spatially) the water and solute dynamics of this heterogeneous system using soil solution sampling, high temporal resolution measurements of bulk soil electric conductivity and

* Corresponding author. Tel.: +49 331 288 2119; fax: +49 331 288 2137.

E-mail addresses: jboike@awi-potsdam.de (J. Boike), olaf.ippisch@iwr.uni-heidelberg.de (O. Ippisch), fsppo@uaf.edu (P.P. Overduin), hagedorn@u.washington.edu (B. Hagedorn), kurt.roth@iup.uni-heidelberg.de (K. Roth).

¹ Fax: +49 6221 54 4404.

² Tel.: +1 907 474 2758; fax: +1 907 474 7979.

³ Fax: +1 206 543 0489.

⁴ Fax: +49 6221 54 6405.

36 thermodynamic equilibrium modelling of solution chem-
 37 istry. This, in turn, adds insight to the mechanical dynamic
 38 of the mud boil, and to the discussions on the origin and
 39 formation of these periglacial features.

40 Furthermore, these findings contribute directly to the
 41 European Science Foundation project on ‘Sedimentary
 42 Source-to-Sink-fluxes in Cold Environments’. An un-
 43 derstanding of climate processes and their control on
 44 mass transfer processes, such as subsurface behaviour of
 45 solutes in a mudboil, aids in the understanding of mass
 46 export of cold drainage basins.

47 2. Theories of mud boil formation

48 Mud boils are symmetric surface features in
 49 periglacial environments that have puzzled and fasci-
 50 nated researchers since at least 1900. Early observations
 51 and theories of the origin of patterned ground were the
 52 beginning of exciting research. Washburn (1956) sum-
 53 marized and discussed postulations of 19 separate
 54 mechanisms of formation for non-sorted circles in
 55 particular. These ideas are still central in today’s discus-
 56 sions of patterned ground formation.

57 Mud boils (also known as frost boils, frost scars, mud
 58 circles and mud hummocks), classified as non-sorted
 59 circles, are found in areas where the ground is subject to
 60 seasonal freezing and thawing. They are characterized
 61 by a bare, usually doming round mineral soil center,
 62 surrounded by vegetation. Some of the mechanisms
 63 postulated for their formation are: the sorting of soil
 64 materials based on grain size; convection cell like
 65 cryoturbation; diapir formation or upwellings of lower
 66 soil horizons under pressure (Washburn, 1956). A
 67 review of the main mechanisms involved in cryoturba-
 68 tions was presented by Van Vliet-Lanoë (1991) based
 69 upon field measurements and micromorphological data.
 70 She concluded that “differential frost heaving appears to
 71 be the main mechanism of cryoturbation” (pp. 123) and
 72 that the presence of organics enhances differential frost
 73 heaving. Kessler et al. (2001) modelled sorted circle
 74 formation (with barren finer grained circle centers
 75 surrounded by stones) from two layers distinct in par-
 76 ticle size using a purely mechanical model. The freezing
 77 front pushed soil to more compressible soil regions,
 78 accumulating in soil plugs that reach to the surface.
 79 During thawing, consolidation occurred vertically. The
 80 circle was maintained at the surface by the circulation of
 81 the stone and fine material domains, upward in the circle
 82 center and downward at the edges. Walker et al. (2004)
 83 presented horizontal soil profiles across a mud boil.
 84 Nutrient concentrations (available potassium, phosphor,
 85 nitrogen) and water content declined from the margins

toward the center, a trend which they attributed to more
 ‘mechanical’ activity towards the center of the boil.

2.1. Study site

The Bayelva catchment is located about 3 km from
 Ny-Ålesund, Spitsbergen (78°55’N, 11°E) in the fore-
 field of the Brøggerbreen glacier (Fig. 1A, B). In this
 region, continuous permafrost underlies coastal areas to
 depths of about 100 m and mountainous areas to depths
 greater than 500 m. The North Atlantic Current warms
 this area to mean monthly air temperatures around
 –13 °C in January and 5 °C in July, respectively and
 provides about 400 mm annual precipitation mostly as
 snow between September and May. Our study site is
 located at about 25 m above mean sea level, on top of a
 small hill covered with unsorted circles (Fig. 1C). It is
 not clear if the mud boils on this hill are currently being
 degraded (for example, by gelifluction) or maintained
 by active cryoturbation. Vegetation encroaching from
 the sides into the mud boil’s center – though the centers
 are still doming – is an indicator for slow mass dis-
 placement and semi-active behaviour. While other
 patterned ground phenomena (such as sorted circles
 and stripes) are found in the vicinity of the hill, these
 mud boils are only present on Leirhaugen hill. The mud
 boils were or are formed under local conditions favour-
 able for mud boil formation after the last glacial period.

Leirhaugen hill is mainly composed of rock, but
 partly covered by a mixture of sediments: glacial till,
 finer glacio-fluvial sediments and clay formed by the
 last glacial advance (Tolgensbakk, personal communi-
 cation). The gray color of the sediments suggests that
 the material was deposited by the Kongsfjorden glacier
 and not the adjacent Brøggerbreen glacier, which
 deposits redder material. Marine sedimentation could
 also have contributed since the hill is located below the
 marine limit (about 38 m).

3. Methods

We instrumented one of these non-sorted circles
 (Fig. 1D) in August 1998 to automatically monitor
 hourly temperature and volumetric liquid water content
 (θ). Altogether 32 time domain reflectometry (TDR)
 probes and 32 temperature probes were installed over
 the 1 × 1 m profile. The position of the TDR probes is
 shown in Fig. 2. The TDR and temperature data set
 considered in this study is limited to 1999, the year in
 which suction lysimeter data were collected. During
 installation, soil samples were taken for the analysis of
 physical parameters. The texture and composition of 25

134 samples were determined using standard methods. Wet
 135 soil was passed through a sieve with 63 μm size to
 136 measure sand content. After destruction of organics and
 137 limestone, silt and clay were separated by sedimentation

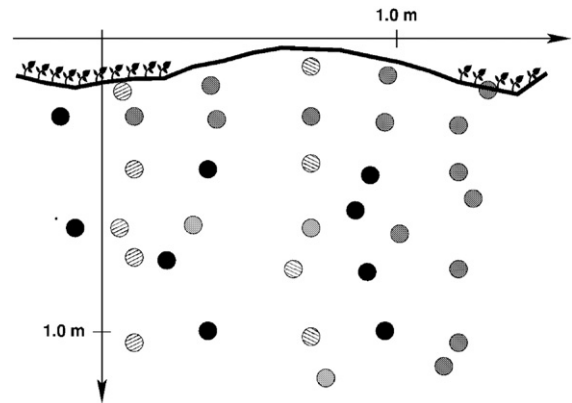
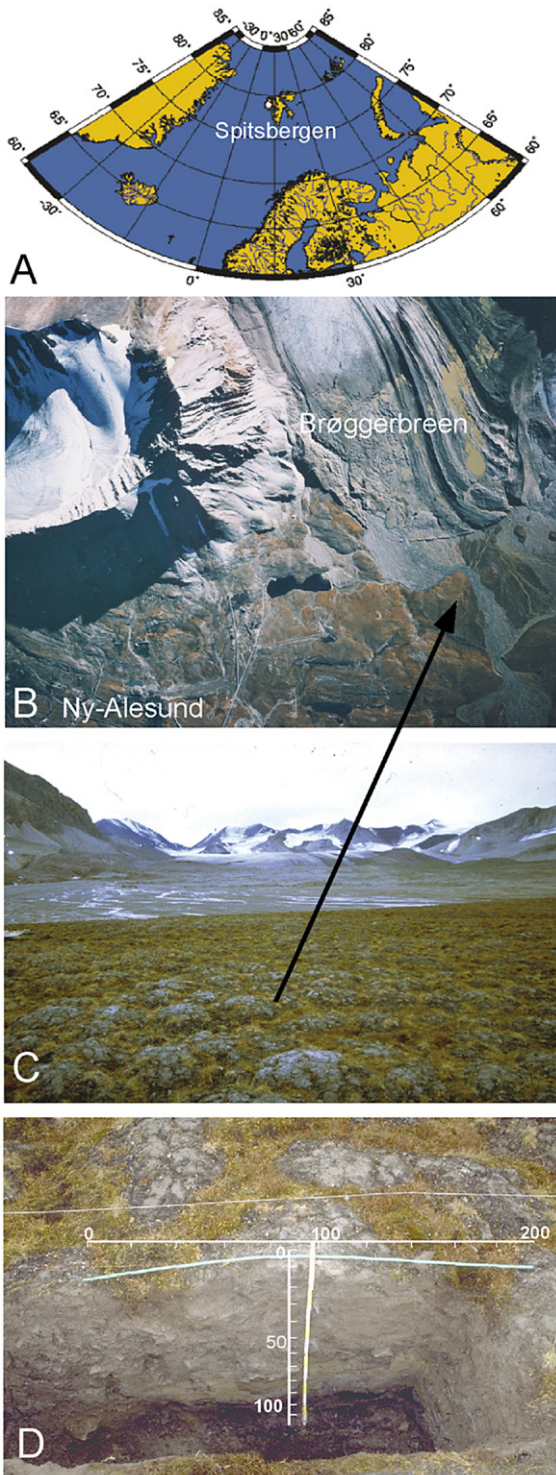


Fig. 2. Position of TDR probes (grey and hatched circles) installed in the mud boil. Temperature probes are installed adjacent to TDR probes. For the analysis, the left profile under vegetation and the profile underneath the center of the mud are used (hatched circles). In addition, nine suction lysimeters (black circles) are installed close to TDR probes (see also Table 1).

in Atterberg cylinders. Soil temperatures were recorded 138
 using thermistors calibrated at 0 °C with a precision of 139
 2.4×10^{-4} °C at 0 °C and an absolute error less than 140
 ± 0.02 °C over the temperature range ± 30 °C. Volumetric 141
 liquid water content was calculated from TDR 142
 measurements with an accuracy of 0.02 to 0.005 and a 143
 precision better than 0.005. Soil water was sampled in 144
 1999 using Prenart® suction cups (5 cm long, pore size 145
 2 μm ; Gravquick, Denmark) cups that were installed in 146
 1998 at different depths close to TDR probes. Soil water 147
 was analyzed in the field for pH, electric conductivity 148
 and alkalinity. The remaining sample water was filtered 149
 and stored at 4 °C in pre-cleaned HDPE bottles until 150
 laboratory analysis took place. Cation concentrations 151
 were analyzed with ICP-OES (Optima 3000 XL, Perkin 152
 Elemer) and anion concentrations were measured with 153
 ion chromatograph (Dionex 320). 154

3.1. TDR and bulk electric conductivity 155

Data on spatial and temporal distribution of water 156
 and solutes in frozen and unfrozen soils are essential for 157
 energy and mass transport models. A fast method to 158
 measure the volumetric water content *in situ* is TDR. 159

Fig. 1. The location of Spitsbergen (A) and aerial picture (1:15000) of the area around Ny-Ålesund (B). The study site (arrow) is located on Leirhaugen hill close to end moraines of the Brøggerbreen glacier. Parts of the road network of Ny-Ålesund can be seen in the lower left part of the picture. The Bayelva study site (C) is located in a field covered with non-sorted circles. The excavated mud boil is shown in D. The bare soil circle centers range about 1 m in diameter and are surrounded by vegetated borders consisting of a mixture of low vascular plants, mosses and lichens.

160 TDR has become a reliable and widely used technique
 161 to measure the water content in frozen and unfrozen
 162 soils (for example, Topp et al., 1980; Patterson and
 163 Smith, 1980; Roth et al., 1990). The TDR technique for
 164 measuring the volumetric water content is based on the
 165 large disparity in the relative dielectric permittivities of
 166 water and the other soil constituents. The bulk relative
 167 dielectric permittivity of the soil determines the velocity
 168 with which an electromagnetic wave travels through the
 169 soil, so that measurement of the travel time for a known
 170 distance allows determination of the material's permit-
 171 tivity. We use a physically-based dielectric mixing

172 model to compute the composite dielectric number of a
 173 multiphase mixture using the relative dielectric permit-
 174 tivities and volume fractions of its constituents (Roth
 175 et al., 1990).

176 TDR can also be used to measure the impedance of the
 177 bulk soil Z (Ω), which is related to the bulk soil electric
 178 conductivity as a function of time. The bulk soil electric
 179 conductivity is directly related to the concentration of ionic
 180 solutes (Reluy, 2004) and hence TDR is suited for *in situ*
 181 detection of well-dissociating solutes. The impedance can
 182 be determined from the attenuation of an electromagnetic
 183 wave traveling along the probe after all multiple

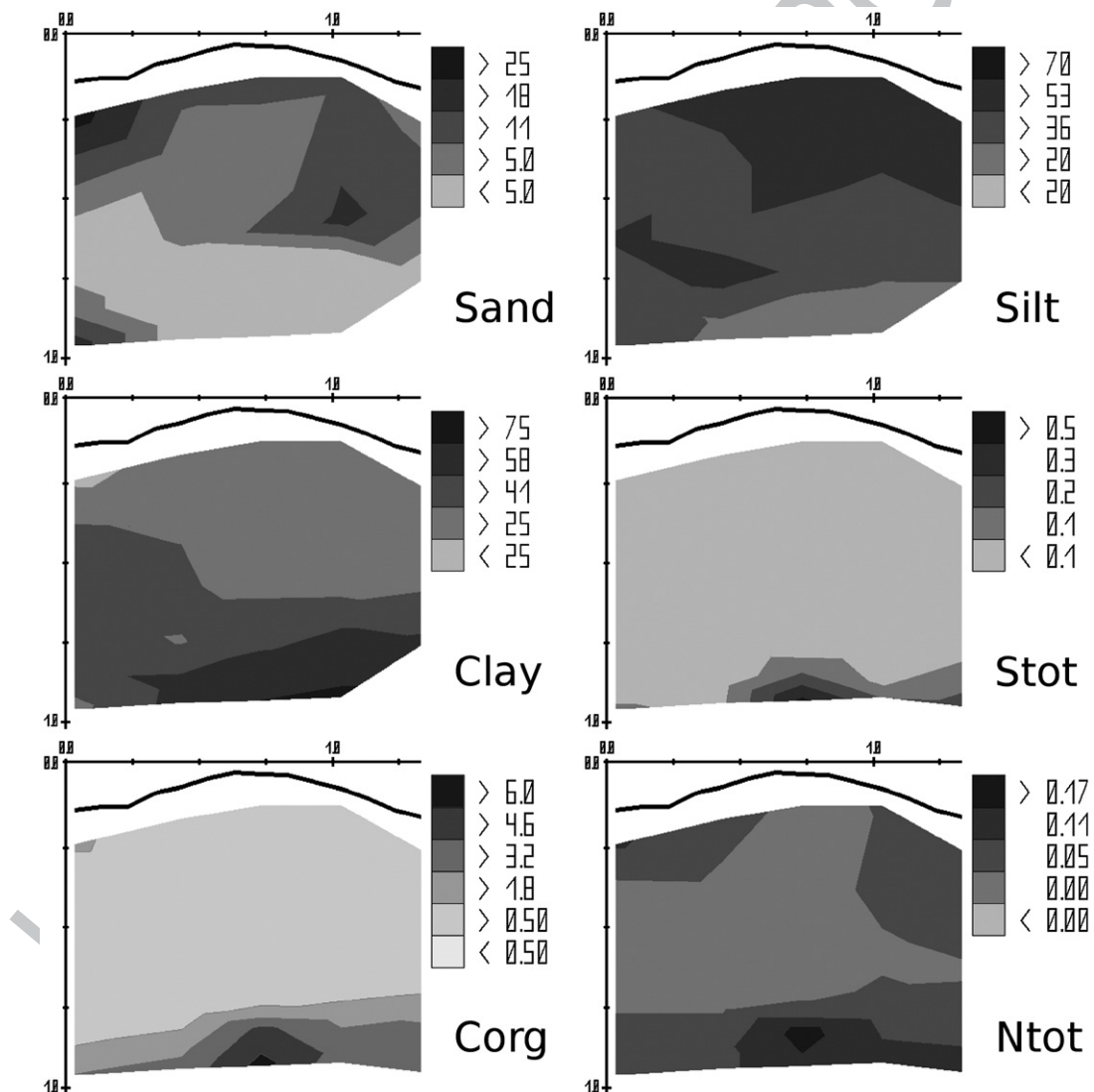


Fig. 3. 2-D distribution of sand, silt, clay and total carbon, nitrogen, sulphur of the mud boil in % weight. Linear interpolation is used between 25 sampling points.

184 reflections have ceased and the signal reaches a stable
185 level. Usually it is assumed that the impedance is related
186 to the bulk soil electric conductivity by:

$$188 \sigma_b^{25} = \frac{K_p}{Z - Z_{cable}} f_T \quad (1)$$

187 where σ_b^{25} [$S m^{-1}$] is the soil bulk electric conductivity
189 corrected to 25 °C, K_p [m^{-1}] is the geometric cell constant
190 of the TDR probe, Z_{cable} [Ω] accounts for the total
191 resistance of cables, connectors and cable tester and f_T [–]
192 is a temperature factor defined as:

$$193 f_T = 1 + \alpha(T - 25) \quad (2)$$

194 where T [°C] is the soil temperature and $\alpha = 0.019 \text{ } ^\circ\text{C}^{-1}$ is
195 the temperature coefficient (Heimovaara et al., 1995). We
196 calibrated our TDR probes in a range of solutions with
197 known electric conductivities, following the method of
198 Heimovaara et al. (1995). As there was no longer a linear
199 relation between measured impedance and the inverse of
200 the conductivity for high concentrations, we modified
201 Eq. (2) to:

$$202 \sigma_b^{25} = \left(\frac{1}{Z - Z_{cable}} - B \right) K_p f_T \quad (3)$$

203 where B is an additional fitting parameter. B , K_p and
204 Z_{cable} were determined by non-linear least squares
205 fitting.

206 3.2. Calculation of soil solution electric conductivity σ_w

207 The relationship between bulk electric conductivity
208 and the electric conductivity of the liquid phase depends
209 on the conductivity of the solid phase and the geometry
210 of the phases, which is related to soil structure and air,
211 ice and water contents. There are several empirical
212 models, partly with some theoretical justification. Boike
213 and Roth (1997) compared the descriptive power of
214 three models for a permafrost site in Siberia by a com-
215 parison of the conductivity measured in water extracted
216 from suction cups with the conductivity predicted from
217 TDR measurements. For the coarse textured soils
218 studied they found the best agreement with a simple
219 regression model:

$$220 \sigma_b = A\theta\sigma_w \quad (4)$$

221 where σ_w [$S m^{-1}$] is the electric conductivity of the soil
222 solution, θ [–] is the volumetric liquid water content of
223 the soil and A [–] is a fitting parameter. For three

different mineral soils the parameter A varied between 224
0.7 and 4.8. Best results were obtained with probe 225
specific calibrations. Furthermore, they suggested that A 226
did not change from frozen to unfrozen soils and that 227
this model may be applied to calculate σ_w for frozen 228
conditions as well. To our knowledge, the only other 229
model predicting σ_w from TDR-determined σ_b in frozen 230
soils was introduced by van Loon et al. (1991; also 231
reviewed in Boike and Roth, 1997). This model has 232
been applied for the study of solute dynamics in 233
Swedish field soils (Lundin and Johnsson, 1994) and 234
in frozen lab columns (Stähli and Stadler, 1997) without 235
prior calibration to soil solution electric conductivity. As 236
the model by van Loon et al. (1991) did not predict 237
solution electric conductivity as well as the regression 238
model for permafrost soils in Siberia (Boike and Roth, 239
1997) we did not consider this model further in this 240
study. 241

242 4. Results

Soil composition data from the 25 samples taken 243
from the profile is presented in Fig. 3. The soil material 244
generally consists of silty clay with some larger stones. 245
The silt content decreases from over 50% at the top of 246
the profile to less than 30% at the bottom, concomitant 247
with an increase of clay content to over 50% (Fig. 3). 248
Concentrations of organic carbon, total nitrogen and 249
total sulphur are highest at the bottom of the profile, 250
peaking below the mud boil center. Of note are 251
especially high concentrations of organic carbon (>6% 252

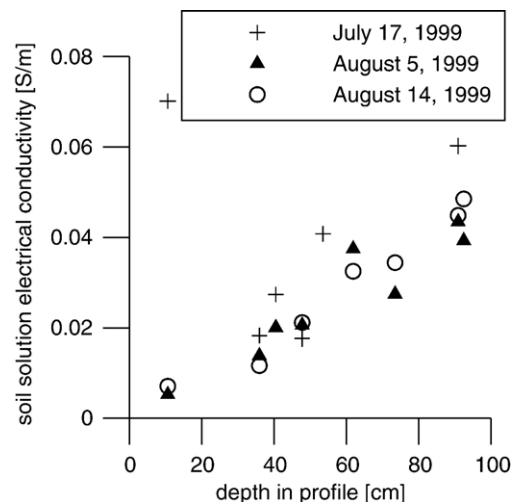


Fig. 4. Soil water electric conductivity obtained from suction lysimeter water at three different times over depth.

weight) at the bottom of the profile. Nitrogen is also elevated below the vegetated trough of the profile.

4.1. Determination of σ_w

The bulk electric conductivity of the soil is generally considered to be the sum of the conductive contributions of the liquid phase and the soil matrix surface

$$\sigma_b = \sigma_w + \sigma_s \quad (5)$$

The matrix surface contribution is generally assumed to be low relative to that of the soil solution, and is often neglected (Boike and Roth, 1997). The texture of the soil in this study site is finer and has far more clay than the coarse textured soils studied by Boike and Roth (1997). Since the clay content is high, the conductivity of the solid phase may no longer be negligible and it is not clear if these findings are also valid for this site. To verify this and to calibrate the measurement of σ_w we used the measured electric conductivity of water extracted on three dates (July 17, August 5 and 14, 1999) from suction cups installed at nine positions near the TDR probes (Fig. 4). The electric conductivity of the extracted water increased with increasing profile depth, thus the rise of bulk electric conductivity cannot be attributed solely to the increase in finer soil particles.

Suction lysimeter data were used to calibrate the model (Eq. (4)). The calculated mean A factors for the regression model are given in Table 1. Calculated A values lie within the same range as the ones calculated by Boike and Roth (1997). Fig. 5 shows a comparison of σ_w measured in soil water and the corresponding σ_w calculated from TDR measurements. Altogether we can see a good linear relation with some outliers. The two water samples with high concentrations were collected during the first sampling and have different ion composition, as will be explained later in the Discussion

Table 1
Mean calculated A factors for the linear regression model

Suction lysimeter	Suction lysimeter location depth [cm]	A factor	No. of water samples	pH
B1	91	1.1	4	Neutral, pH=7.1
B2	93	1.0	3	Acidic, pH=4.1
B3	62	2.4	4	Alkaline, pH=7.8
B4	74	2.8	2	Neutral, pH=7.1
B5	48	4.0	5	Alkaline, pH=7.9
B6	54	1.6	3	Alkaline, pH=8.1
B7	36	4.7	6	Alkaline, pH=7.5
B8	41	3.8	4	Alkaline, pH=8.0
B9	10	4.0	3	Neutral, pH=6.7

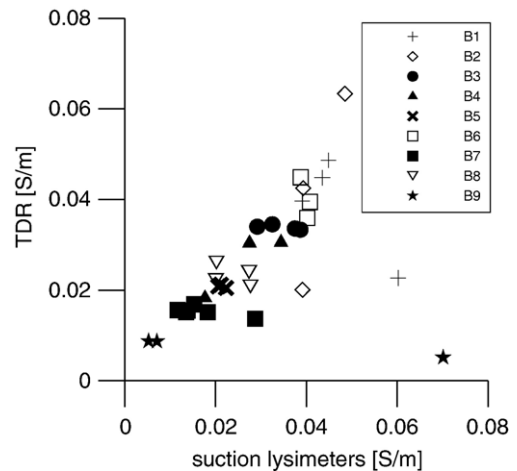


Fig. 5. Soil water electric conductivity obtained from suction lysimeters (names of suction lysimeters in legend) compared to values calculated from bulk electric conductivity (TDR probes) using model (4).

A closer examination of the values for individual probes shows a narrow range of conductivities covered by the limited amount of samples taken, so that within the accuracy of the measurements they represent one data point for each probe. This makes verification of the model difficult. However, we assume that there are monotone relations between σ_w and σ_b and θ and σ_b . Therefore the qualitative behaviour of σ_w derived from the TDR measurements is expected to be correct even if absolute errors are introduced by disregarding the conductivity of the solid phase.

4.2. Temperature, volumetric water content and soil solution electric conductivity dynamics

For the following analysis, we chose two profiles: one located below the vegetated left trough and the other one below the center of the mud boil (Fig. 2).

Fig. 6 shows rainfall and snow depth, soil temperature, soil volumetric water content and σ_w at 4 different depths below the vegetated trough. As expected, the probe closest to the surface (0.06 m) shows higher temperatures and daily temperature fluctuations compared to the lower probes. The temperature signal is attenuated with depth. In May, the snow liquid water content increases considerably, a process also enhanced by rain on snow events (Boike et al., 2003), and infiltration of water rapidly warms the soil at all depths. This is reflected in Fig. 6 by the dramatic increase in the volumetric water content of the soil at successive depths. The liquid water content mirrors most clearly the advance of the thaw front. The phase change ice/water starts during snow ablation and is much enhanced after the snow has ablated. The soil

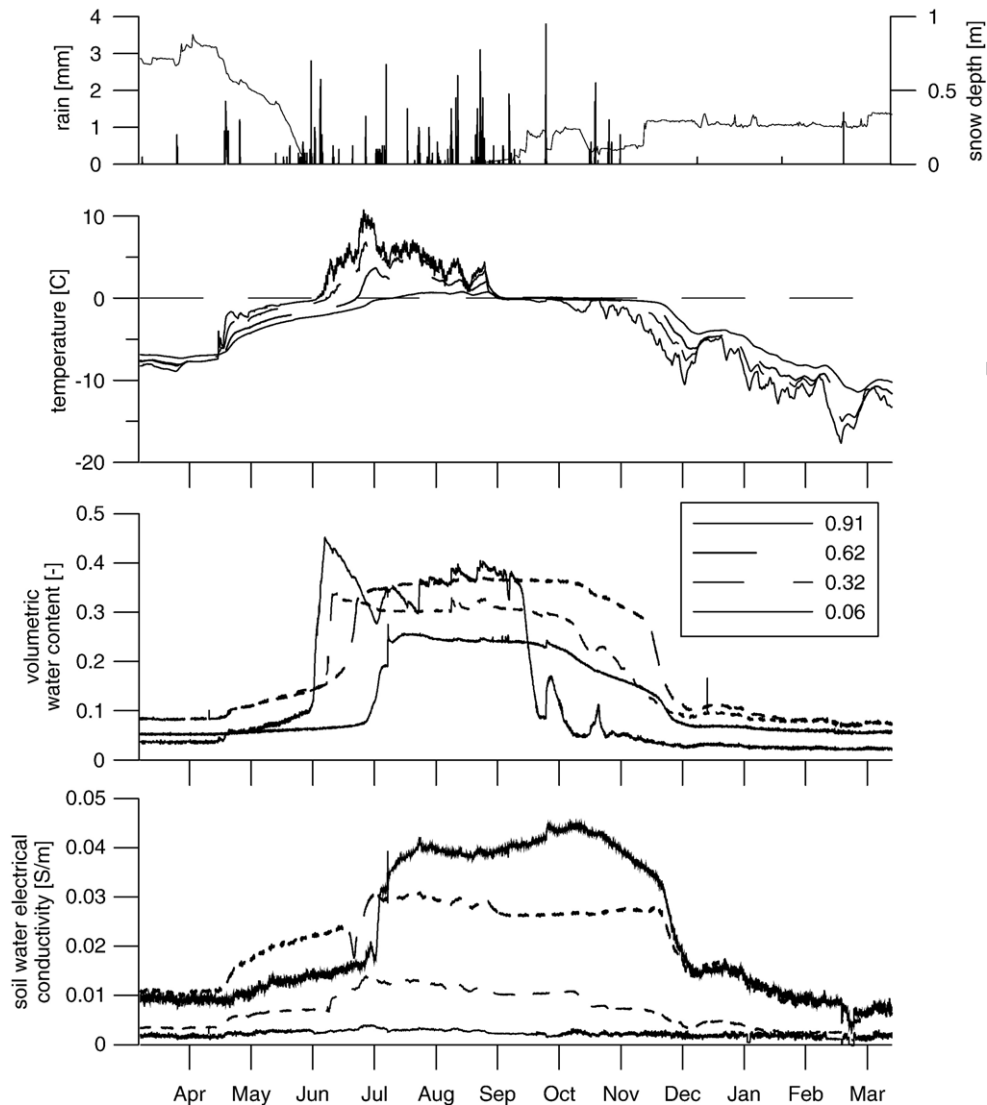


Fig. 6. Rainfall and snow depth, soil temperatures, soil water content and soil water electric conductivity from April 1999 to April 2000 at four depths for a profile underneath the vegetated cover.

319 temperature sensor at 0.91 m depth passes 0 °C around the
 320 end of July. However, low volumetric water contents
 321 (~0.25) that remain constant over the summer indicate
 322 that the soil is not completely thawed. The temperature
 323 sensor at 1.22 m depth (not shown in diagram) indicates
 324 that the soil never thaws at this depth. During the summer,
 325 volumetric water content remains constant at 0.62 m
 326 depth, indicating the perched water table above the frozen
 327 ground. Once freezing starts in September, soil tempera-
 328 tures at all depths drop to below zero and phase change
 329 from water to ice is initiated (“zero curtain effect”). The
 330 phase change is completed by mid-November, after which
 331 the soil profile cools. The volumetric liquid water content
 332 in these frozen soils during winter ranges between 4 and

9% and is lowest at the surface due to desiccation (vapour
 migration out of the soil, see Roth and Boike, 2001).

The general seasonal behaviour of σ_w below the
 organic (except for the probe nearest to the surface at
 0.06 m) can be summarized as follows: increase of σ_w
 during thawing, highest concentrations during the summer
 and decrease during fall phase change. However, during
 the spring thaw, the behaviour of σ_w is different
 for each soil depth. At intermediate depth (0.32 m), σ_w
 increases during thaw, but continues to increase even
 after the soil is completely thawed, indicating either
 transport of solutes to this area or local and continued
 increases in the concentration of charged solutes. At
 0.62 m depth, a pronounced drop in conductivity occurs

347 during thaw at about 15% liquid water content, which
 348 indicates that dilution of the soil water has occurred,
 349 probably via downward migration of meltwater with
 350 lower concentrations of dissolved ionic species. In ad-
 351 dition, this is the soil depth with the highest σ_w in the
 352 frozen soil. Since this is the soil depth that remains
 353 thawed longest in the fall (Boike et al., 2003), migration
 354 of excluded ions would take place towards this depth.
 355 This is also suggested by a small increase of θ and σ_w in
 356 December after closure of the zero curtain.

357 Throughout the whole summer σ_w is relatively stable,
 358 with small increases of σ_w occurring at the three
 359 intermediate depths simultaneously with an increase of
 360 θ after a series of rain events during the latter half of

361 August. However, there is also a peak in σ_w measured 361
 362 with the deepest probe at the end of July, which is not 362
 363 connected to a corresponding increase of water content. 363
 364 Only the surface probe shows an increase in θ at this time, 364
 365 caused by a minor rain event. As the same peak can be 365
 366 recognized at the deepest probe below the mud boil 366
 367 center, it is unlikely to be an artefact and either an *in situ* 367
 368 increase in solute concentration, for example by dissolution 368
 369 of salts, or lateral inflow must have occurred. 369
 370 Generally in the thawed organic profile, soil water 370
 371 conductivity increases with depth and the highest concen- 371
 372 trations occur at the bottom of the profile (0.91 m). 372

373 In the barren soil below the center of the boil the 373
 374 fluctuations of temperature, water content (Fig. 7) and σ_w 374

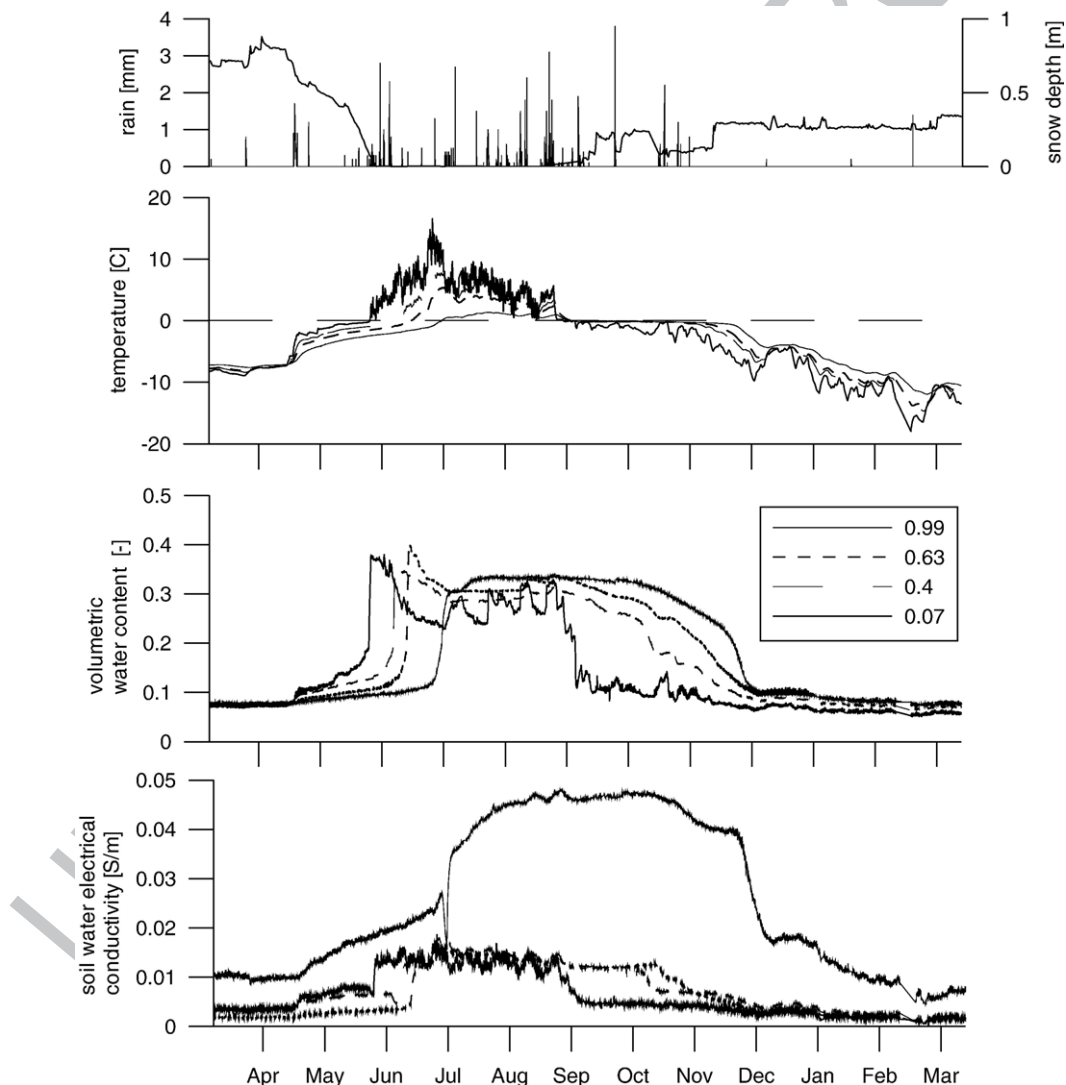
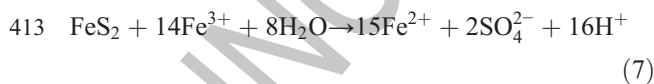


Fig. 7. Rainfall and snow depth, soil temperatures, soil water content and soil water electric conductivity from April 1999 to April 2000 for profile underneath mud. $A=3.8$ in Eq. (4) was used for TDR probe at 0.07 m under mud.

375 near the surface are generally higher than below the
 376 vegetation covered trough. Due to the lack of vegetation,
 377 the profile thaws earlier. In mid-July, the thaw front passes
 378 the probe at 0.99 m depth. Over the course of the summer,
 379 the center of the mud boil thaws to greater depth com-
 380 pared to the vegetated trough. The water content of the
 381 soil surface layer shows greater fluctuations in response to
 382 wetting by rainfall and subsequent drying since these
 383 processes are not buffered by vegetation. The σ_w values
 384 increase with depth in a fashion similar to the profile
 385 under the vegetated trough, with highest values of σ_w at
 386 the bottom of the boil and, σ_w values are generally higher
 387 at the bottom of the mud profile. Decreases in σ_w from the
 388 beginning of June (0.07 m) until the middle of July
 389 (0.99 m) in the mineral profile indicate the dilution of the
 390 soil solution by downward migration of meltwater. As
 391 observed for the organic profile, these decreases in soil
 392 solution electric conductivity are associated with thawing,
 393 but occur before the liquid water content increases.

394 Soil waters from deep suction lysimeters B1 and B2,
 395 and from shallower lysimeters B5 and B6, were analyzed
 396 for cation and anion concentrations. Based on lysim-
 397 eters B6 and B5 (about 60 cm), the most concentrated
 398 cations are HCO_3^- and Mg^{2+} followed by $\text{Ca}^{2+} >$
 399 $\text{Si} > \text{SO}_4^{2-} > \text{Cl}^- > \text{K}^+ > \text{NO}_3^-$. Ionic concentrations at B6,
 400 beneath the center of the mud boil are generally higher
 401 than at B5, beneath the vegetated trough, with exception
 402 of NO_3^- and Si_{aq} . The deeper soil solutions (around
 403 100 cm) are closer to the permafrost table and were
 404 most concentrated in SO_4^{2-} , followed by $\text{Mg}^{2+} > \text{Ca}^{2+} >$
 405 $\text{HCO}_3^- > \text{Si}_{\text{aq}} = \text{K}^+ = \text{Cl}^-$. The first samples collected from
 406 B2 in July 1999 show very low pHs of 4, higher Fe_{aq}
 407 ($20\text{--}40 \mu\text{g L}^{-1}$) and very high Al_{aq} ($1\text{--}2 \text{mg L}^{-1}$)
 408 concentration compared to later samples. A possible
 409 inorganic mechanism leading to such a low pH in natural
 410 water is dissolution of pyrite. Two possible overall redox
 411 reactions are given below (Langmuir, 1997, pp. 458):



416 This reaction needs electron acceptors that can either
 417 be provided by oxygen or by an abundance of Fe^{3+} .
 418 Although this reaction would explain both high sulphate
 419 concentrations and low pH, more details (e.g. redox
 420 potential) are required to reveal if oxidation and
 421 dissolution of pyrite is the reason for the low pH values.
 422 During excavation of this and another soil pit coal
 423 fragments were found and exploratory excavations for

424 coal are located nearby. The low pH, occurrence of coal
 425 and enrichment in Fe all support dissolution of pyrite
 426 as a common cause. The low pH enhances chemical
 427 weathering and therefore contributes to the overall in-
 428 crease in solute concentration at depth.

429 The rapid decrease in σ_w when soils freeze (Figs. 6
 430 and 7) is counter-intuitive, since an increase in con-
 431 centration due to the exclusion of ions during freezing is
 432 expected. A first approach to model the change in solute
 433 composition and concentration of soil water at sub-
 434 freezing temperatures can be performed with geochemi-
 435 cal equilibrium model FREZCHEM62 (Marion and
 436 Grant, 1994). This program is written to model changes
 437 in chemistry during stepwise freezing of a water solution
 438 and considers either continuous contact between solu-
 439 tion and precipitated phase or fractional removal of
 440 precipitated phase from solution. It does not incorporate
 441 soil physical factors like mineral, organic or colloid
 442 surfaces that most likely contribute to changes in
 443 water chemistry. However, it allows estimation of the
 444 chemical development of a solution during freezing.
 445 Results of the modelling with FREZCHEM of solutions
 446 B1 and B6 collected at 1 and 0.6 m depth is shown in
 447 Fig. 8. Liquid water content rapidly decreases below
 448 subfreezing temperatures and at $-5 \text{ }^\circ\text{C}$ only 0.006% of
 449 the total water content present before freezing is still
 450 unfrozen. During freezing salts of different composition
 451 precipitate from solution in the sequence: $\text{CaSO}_4 \cdot 2\text{H}_2\text{O}$,
 452 MgCO_3 , $\text{CaMg}(\text{CO}_3)_2$, K_2SO_4 , and $\text{Na}_2\text{SO}_4 \cdot 10\text{H}_2\text{O}$.
 453 The precipitation of these salts causes the changes in
 454 molar elemental ratios displayed in Fig. 8. The most
 455 striking difference between the soil solution with high
 456 SO_4^{2-} concentration (B1, B2) and high HCO_3^- concen-
 457 tration (B6) is in the change of Na/Cl ratios. While in the
 458 B1 soil solution the Na/Cl ratio constantly increases, it
 459 decreases in B6 due to the formation of KCl at $-10 \text{ }^\circ\text{C}$.
 460 Compared to TDR measurements, the calculated liquid
 461 water content based on water chemistry is much lower, a
 462 difference amounting to up to 9% by volume. An im-
 463 portant part of liquid water in frozen soils exists as thin
 464 water films on particle surfaces (Ugolini and Anderson,
 465 1973), and such water–surface interactions are not
 466 considered in FREZCHEM. If surface-bound water is
 467 not in contact with the solute-rich solution excluded
 468 from the forming ice, then the predicted precipitation of
 469 salts due to freezing would hold. Measurements of σ_w
 470 depend on a direct current pathway between electrodes
 471 (in this case, TDR sensor wave guides), so that isolated
 472 pockets of high concentration will not contribute to the
 473 measured bulk electric conductivity of the soil. Surface
 474 bound water, however, contributes to the measurement
 475 of σ_b (Guy–Chapman double layer theory).

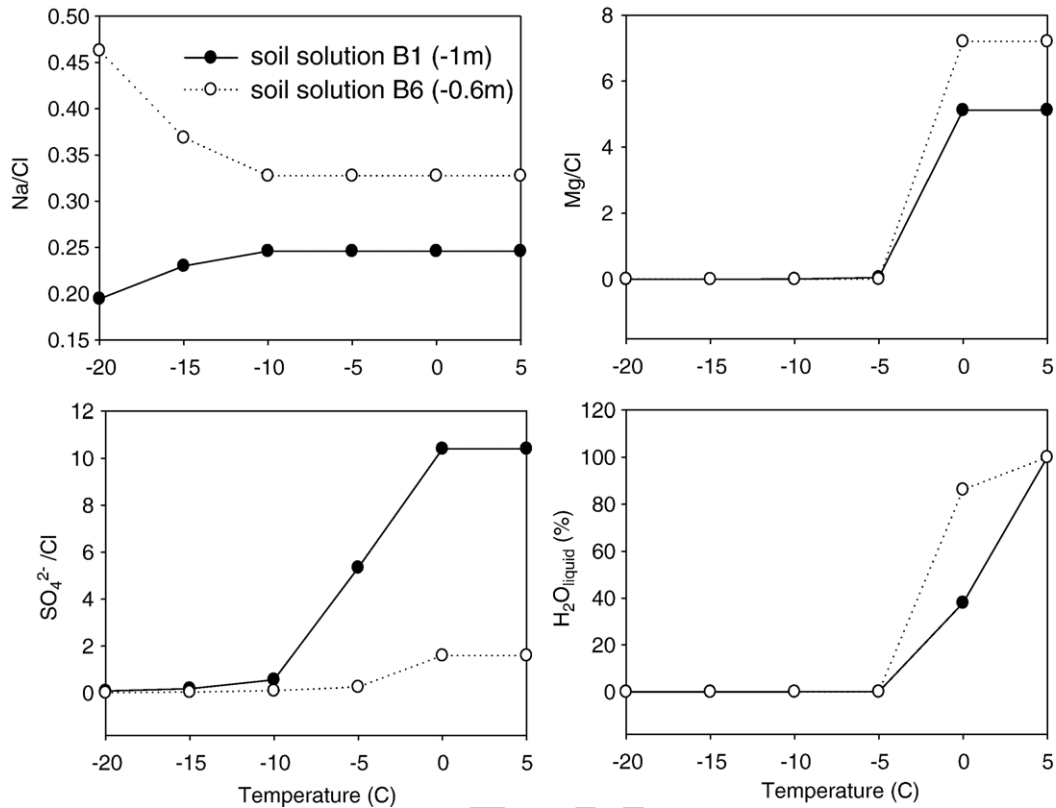


Fig. 8. Molar element ratios and liquid water concentration (%) modelled with FREZCHEM62 between +5 and –20 °C. The soil solutions are taken from suction cups B6 and B1. Changes in element ratios indicate formation of solid salt precipitates that remove specific elements from solution. Liquid water content refers to percent of liquid water of total amount of water that was present before freezing. At –20 °C liquid water content is less than 1‰.

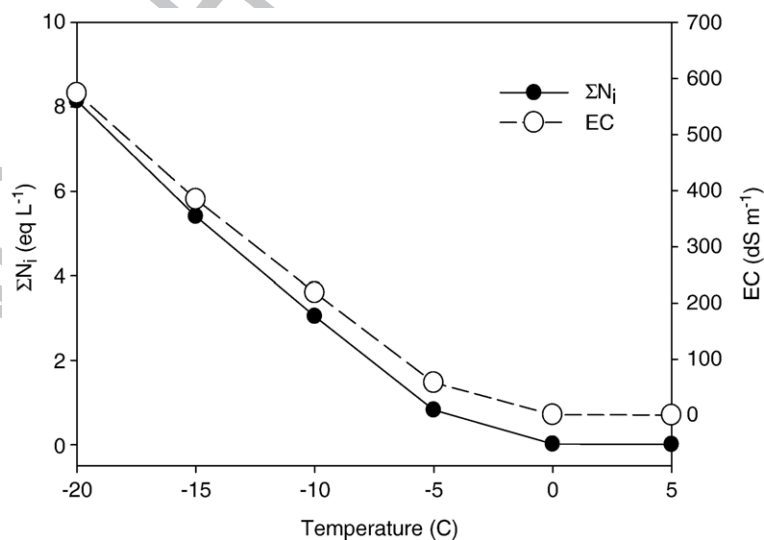


Fig. 9. Calculated total ion concentration in eq L⁻¹ in remaining solution during freezing. EC is calculated from Eq. (8) using total ion activity (eq/L) ($\Sigma a_i = \Sigma N_i \gamma_i$; where γ_i is the activity coefficient provided by FREZCHEM62) instead of ion concentration N_i .

476 To compare the modelled solution with measured
 477 conductivity, the electric conductivity is calculated
 478 following the approach of Reluy et al. (2004) relating
 479 electric conductivity (EC) to the equivalent concentra-
 480 tion of ions in solution ($\sum N$). The relation between EC
 481 and $\sum N$ is given by:

$$482 \quad EC = 10^{-6} u' F \sum_i N_i \quad (8)$$

483 where F is Faraday's constant (Cmol^{-1}), and u' is the
 484 concentration-weighted mean equivalent mobility:

$$485 \quad u' = \frac{\sum_i N_i u_i}{\sum_i N_i} \quad (9)$$

486 where u_i is the limiting equivalent ionic mobility of ion i
 487 [$\text{mS cm}^2 \text{ mol eq}^{-1} \text{ C}^{-1}$]. In our calculation we used values of u_i
 Q2 488 ~~given in Table 3 in Reluy et al. (2004).~~ Instead of
 489 normalities, N_i , we used the activities calculated with
 490 FREZCHEM for each ion and ion pair. The results of this
 491 calculation are shown in Fig. 9, indicating that the solution
 492 electric conductivity increases with increasing solute
 493 concentration from around 0.05 S m^{-1} to 60 S m^{-1} .
 494 The total concentration of ions in the remaining unfrozen
 495 solution increases by a factor of ~ 1000 , whereas without
 496 precipitation of salts the concentration would increase by a
 497 factor of ~ 17000 at the final water content. Modelled
 498 changes to soil solution, in the absence of mineral–soil
 499 solution interactions, lead to a predicted increase in soil
 500 water electric conductivity of three orders of magnitude
 501 with freezing. The water electric conductivities in the
 502 thawed soil estimated for the solution analyzed here are of
 503 the same order of magnitude as those predicted by this
 504 model (e.g. for a measured solution electric conduc-
 505 tivity of 0.038 S m^{-1} , we predict an electric conductivity
 506 of 0.050 S m^{-1}).

507 If the contribution of the clay particle surface
 508 conductivity to σ_b is significant, the isolation of clay
 509 particles by ice layers could be another reason for the
 510 reduction of σ_b . In that case σ_w in frozen soil might be
 511 underestimated by the values calculated from bulk
 512 electric conductivity measured with the TDR probes.

513 5. Discussion

514 5.1. Observed changes in soil water electric conductivity 515 with time

516 ~~Changes in estimated soil water electric conductivity~~
 517 ~~respond~~ to freezing, thawing and summer rainfall

518 events. Using the model of Boike and Roth (1997),
 519 we show that the largest annual increase and decrease
 520 are associated with thawing and freezing, respectively,
 521 of the soil. During thaw, for both soils under the boil and
 522 the vegetated trough, soil water electric conductivity at
 523 all depths decreases by up to 30% before the increase
 524 associated with thawing occurs. The thaw increase
 525 occurs simultaneously with the increase in liquid water
 526 content associated with the phase change of ice to water.
 527 We suggest that the initial decrease in electric
 528 conductivity indicates that the infiltration and refreezing
 529 of snow meltwater has diluted the available soil
 530 solution.

531 5.2. Increase in solute concentration with depth

532 Our data show that soil solutes within the mud boil
 533 are stratified horizontally throughout the year and that
 534 this stratification, with highest concentrations at the
 535 bottom of the profile, is dominant over any vertical
 536 stratification (org. ~~versus~~ mud). Lundin and Johns-
 537 son (1994) also found that σ_w increased with depth and
 538 percentage of fines in Swedish agricultural soils.
 539 Alekseev et al. (2003) and Kokelj and Burn (2003)
 540 also find the highest concentrations in the soil profile at
 541 the boundary between seasonally thawed soil and
 542 permafrost. Alekseev et al. (2003) conclude that
 543 permafrost landscapes in general accumulate solutes at
 544 the upper boundary of the permafrost, ~~acting~~ as a
 545 geochemical barrier.

546 In addition to this depth stratification, we observe a
 547 slight increase in soil electric conductivity beneath the
 548 center of the mud boil. Depressions, as in our case the
 549 bowl-shaped region beneath the mud boil, have even
 550 higher concentrations of solutes. These subtle variations
 551 in concentration might be the initiator of irregularities in
 552 the permafrost table due to the depression of the freezing
 553 point and thus, the precursor of certain patterned
 554 ground, such as these non-sorted circles. Once a bowl-
 555 shaped depression of the permafrost table exists, cell-
 556 like circulation pattern within the active layer can be
 557 initiated (i.e. the equilibrium model after Mackay,
 558 1980). However, Fig. 8 shows that the depression of
 559 the freezing point by solute exclusion from a freezing
 560 solution with the chemistry of extracted soil water is
 561 only sufficient to maintain less than 0.1 mL of water in
 562 the liquid state per liter of soil solution below $-10 \text{ }^\circ\text{C}$,
 563 implying that the effect of solute exclusion on the
 564 permafrost table depth are minimal compared to those of
 565 differences in surface cover and overlying soil thermal
 566 properties. ~~Therefore it seems plausible that differential~~
 567 ~~frost heave is responsible~~ for the formation of the mud

boils as also stated by Van Vliet-Lanoë (1991). Walker et al. (2004, pp. 178) postulated that frost boils typical of coastal areas pump solutes to the surface as a result of relatively high evaporation rates and that the salts thus deposited inhibit vegetation growth. In contrast to these findings, our data suggest that net accumulation of solutes occurs at the base of the active layer, with little difference between mud boil and adjacent vegetated regions. In both profiles, the highest values of σ_w occur at depth, whereas the lowest values are found in the upper coarser horizon.

The increase with depth probably results from one or both of two general processes. First, seasonal freezing may lead to a cumulative downward migration of solutes as a result of solute exclusion from the freezing soil water. This downward migration is ultimately limited by the presence of the permafrost table, which provides a natural boundary to downward percolation. Secondly, the fraction of finer material increases with depth at this site providing a higher surface area susceptible for chemical weathering.

5.3. Comparison to thermodynamically modelled freezing

The high temporal resolution of soil water electric conductivity data derived from TDR measurements permits qualitative identification of processes such as dilution (melting of pure ice) concentration in frozen soil during snow ablation and migration in the thawed soil. These are in congruence with the observed hydrologic and thermal dynamic. However, the absolute concentration values during the frozen period are much lower than expected if exclusion of solutes from the freezing soil solution occurs, despite the fact that thermodynamically modelled freezing indicates that several salts precipitate from soil solution during freezing. The time difference between the increase in water content and soil water electric conductivity during thawing might indicate kinetic delay of re-dissolution of these salt crystals. Furthermore, some of precipitates, like carbonates and Ca-sulfates, may not re-dissolve completely. The higher amount of particulate inorganic carbon found at depth of mud boil may be a direct result of precipitation of fine carbons combined mechanical movement of fines to bottom of mud boil. The contribution of solute movement is unlikely since it would be against the concentration gradient.

The calculation of electric conductivity from salt concentration and salt composition strongly depends on ion mobility. However, values used for u_i have been determined for temperate solutions. Subfreezing temperatures and changes in the viscosity of water may decrease

ion mobility and electric conductivity. Further experimental investigations are needed to determine mobilities of single ions and ion pairs at temperature below 0 °C. Furthermore, water bound to clay particle and ice surfaces may have lower solute concentrations than regions containing solutes excluded from freezing pore water, leading to lower overall measured salt concentration per unit volume of soil. Ostroumov et al. (2001) found that liquid drops on the surface of the forming ice were probably responsible for solute transport in frozen deposits close to the freezing front. The implication is that excluded solutes are restricted to small, unconnected domains within the soil that would not contribute to measured bulk soil electric conductivity.

5.4. Implications for cryoturbation

Walker et al. (2004) hypothesize that particles and dissolved organic material are carried downward at the margins of frost boils by soil movement attaching, whereas organics accumulate in the thawed of the frost boil. At the center of the mud boil, upward migration of organics occurs. The high concentrations (>6%) of organic carbon in our mud boil (Fig. 2) support their hypothesis. The differences in thermal and hydrologic regime, thaw depth, and total nitrogen, organic carbon and total sulfur concentrations between mud and vegetated trough profiles create a physically different environment. This, in turn, affects the vegetation and possibly governs the mechanical forces that create the mud boils. Cryoturbation is the most effective process in moving organics and (weathered) minerals upwards from the bottom of the active layer, thus counteracting the downward fluxes. Cryoturbation is likely to change with a changing climate. On Svalbard, mean annual ground surface temperature currently increases at a rate of ~0.4 °C per decade (Isaksen et al., 2001).

6. Conclusion

The influence of mud boils on solute migration is small compared to the influence of the seasonal freeze–thaw cycle in the presence of permafrost. The soil solution electric conductivity increases with depth beneath a mud boil, irrespective of lateral position, but seasonal changes in conductivity between frozen and thawed soil are up to 5 times greater. TDR-determined bulk electric conductivity is a useful tool, since it permits high temporal resolution measurement of changes in soil electric conductivity, and thus a means of investigating solute dynamics. The deviation between TDR determined and thermodynamically modelled changes in soil solution chemistry

666 identifies two future research goals: (i) a new model
667 accounting for changes in phase geometry during freezing
668 and (ii) including the effects of soil surface physics in
669 thermodynamic models of freezing.

670 Acknowledgements

671 We gratefully acknowledge financial support from
672 the Deutsche Forschungsgemeinschaft (DFG), the
673 European Union and a research grant awarded to Julia
674 Boike by the Deutsche Akademie der Naturforscher
675 Leopoldina. Essential logistic and technical support was
676 provided by the German and the Norwegian Research
677 Stations in Ny-Ålesund and by Christian Wille and
678 Molo Stoof. Thanks to Antje Eulenburg for analyzing
679 the water samples. Discussions with Hugh French
680 during the 2nd Workshop Shifting Lands – New
681 Insights Into Periglacial Geomorphology in France –
682 motivated this contribution.

683 References

- 684 Alekseev, A., Alekseeva, T., Ostroumov, V., Siegert, C., Gradusov, B.,
685 2003. Mineral transformation in permafrost-affected soils, North
686 Kolya Lowland, Russia. *Soil Sci. Soc. Am. J.* 67 (2), 596–605.
- 687 Boike, J., Roth, K., 1997. Time domain reflectometry as a field method
688 for measuring water content and soil water electrical conductivity
689 at a continuous permafrost site. *Permafr. Periglac. Process.* 8 (4),
690 359–370.
- 691 Boike, J., Roth, K., Ippisch, O., 2003. Seasonal snow cover on frozen
692 ground: energy balance calculations of a permafrost site near Ny-
693 Ålesund, Spitsbergen. *Geophys. Res.* 108 (D2), 8163. doi:10.1029/
694 2001JD000939.
- 695 Heimovaara, T.J., Focke, A.G., Bouten, W., Verstraten, J.M., 1995.
696 Assessing temporal variations in soil water composition with time
697 domain reflectometry. *Soil Sci. Soc. Am. J.* 59, 689–698.
- 698 Isaksen, K., Holmlund, P., Sollid, J.L., Harris, C., 2001. Three deep
699 alpine permafrost boreholes in Svalbard and Scandinavia. *Permafr.*
700 *Periglac. Process.* 12, 13–25.
- 701 Kessler, M.A., Murray, A.B., Werner, B.T., Hallet, B., 2001. A model
702 for sorted circles as self-organized patterns. *J. Geophys. Res.* 106
703 (B7), 13,287–13,306.
- 704 Kokelj, S.V., Burn, C.R., 2003. Ground ice and soluble cations in near-
705 surface permafrost, Inuvik, Northwest Territories, Canada. *Permafr.*
706 *Periglac. Process.* 14, 275–289.
- 707 Langmuir, D., 1997. *Aqueous Environmental Geochemistry*. Prentice-
708 Hall, Upper Saddle River, New Jersey. 600 pp.
- 709 Lundin, L.-C., Johnsson, H., 1994. Ion dynamics of a freezing soil
710 monitored in-situ by time domain reflectometry. *Water Resour.*
711 *Res.* 30 (12), 3471–3478.
- Mackay, J.R., 1980. The origin of hummocks, western Arctic coast. 712
Can. J. Earth Sci. 17 (8), 966–1006. 713
- Marion, G.M., Grant, S.A., 1994. FREZCHEM: A chemical- 714
thermodynamic model for aqueous solutions at subzero tempera- 715
tures. Hanover, NH, Cold Regions Research and Engineering 716
Laboratory, U.S. Army Corps of Engineers. 717
- Ostroumov, V., Hoover, R., Ostroumova, N., Van Vliet-Lanoë, B., 718
Siegert, C., Sorokovikov, V., 2001. Redistribution of soluble com- 719
ponents during ice segregation in freezing ground. *Cold Reg. Sci.* 720
Technol. 32, 175–182. 721
- Patterson, D.E., Smith, M.W., 1980. The use of time domain 722
reflectometry for the measurement of unfrozen water content in 723
frozen soils. *Cold Reg. Sci. Technol.* 3, 205–210. 724
- Reluy, F.V., de Bécares, J.M., Hernández, R.D., Díaz, J.S., 2004. 725
Development of an equation to relate electric conductivity to soil 726
and water salinity in a Mediterranean agricultural environment. 727
Aust. J. Soil Res. 42, 381–388. 728
- Romanovskii, N.N., 1996. Periglacial processes as geoindicators in 729
the cryolithozone. In: Berger, A.R., Jans, W.J. (Eds.), *Geoindica-* 730
tors: Assessing Rapid Environmental Changes in Earth Systems. 731
Rotterdam, Balkema. 47–68 pp. 732
- Roth, K., Boike, J., 2001. Quantifying the thermal dynamics of a 733
permafrost site near Ny-Ålesund, Svalbard. *Water Resour. Res.* 37 734
(12), 2901–2914. doi:10.1029/2000WR000163. 735
- Roth, K., Schulin, R., Flüher, H., Attinger, W., 1990. Calibration of time 736
domain reflectometry for water content measurement using a com- 737
posite dielectric approach. *Water Resour. Res.* 26 (10), 2267–2273. 738
- Stähli, M., Stadler, D., 1997. Measurement of water and solute 739
dynamics in freezing soil columns with time domain reflectometry. 740
J. Hydrol. 195, 352–369. 741
- Topp, G.C., Davis, J.L., Annan, A.P., 1980. Electromagnetic 742
determination of soil water content: measurements in coaxial 743
transmission lines. *Water Resour. Res.* 3 (16), 574–582. 744
- Ugolini, F.C., Anderson, D.M., 1973. Ionic migration and weathering 745
in frozen Antarctic soil. *Soil Sci.* 115, 461–470. 746
- van Loon, W.K.P., Perfect, P.H., Groenevelt, P.H., Kay, B.D., 1991. 747
Application of dispersion theory to time domain reflectometry in 748
soils. *Transp. Porous Media* 6, 391–406. 749
- Van Vliet-Lanoë, B., 1991. Differential frost heave, load casting and 750
convection: converging mechanism; a discussion of the origin of 751
cryoturbations. *Permafr. Periglac. Process.* 2, 123–139. 752
- Walker, D.A., Epstein, H.E., Gould, W.A., Kelley, A.M., Kade, A.N., 753
Knudson, J.A., Krantz, W.B., Michaelson, G., Peterson, R.A., Ping, 754
C.-L., Reynolds, M.K., Romanovsky, V.E., Shur, Y., 2004. Frost- 755
boil ecosystems: complex interactions between landforms, soils, 756
vegetation and climate. *Permafr. Periglac. Process.* 15, 171–188. 757
- Washburn, A.L., 1956. Classification of patterned ground and review 758
of suggested origins. *Bull. Geol. Soc. Am.* 67, 823–866. 759
- Washburn, A., 1979. *Geocryology — a survey of periglacial processes* 760
and environments. Edward Arnold, London. 406 pp. 761